SRTTU
Journal of Computational and Applied Research in Mechanical Engineering
jcarme.sru.ac.ir
JCARME
ISSN: 2228-7922

Research paper

Numerical study of transient behavior and heat transfer in a phase change material affected by heat transfer fluid flow parameters

Omid Ahmadi, Sahand Majidi* and Pooyan Hashemi Tari

Faculty of Mechanical & Energy Engineering, Shahid Beheshti University, Tehran, Iran

Article info:

Research history:

Received: 07/09/2019
Accepted: 04/05/2020
Revised: 07/05/2020
Online: 09/05/2020

Keywords:

Phase change material,
Numerical simulation,
Thermal storage,
Melting front,
Exergy analysis.

***Corresponding author:**
s_majidi@sbu.ac.ir

Abstract

Phase Change Materials (PCMs) are known to be capable of storing a substantial amount of energy in relatively low volume. Also, since the phase change process occurs in a nearly constant temperature, PCMs are suitable to be used as storage units. The present study focuses on the effect of Heat Transfer Fluid (HTF) flow parameters on heat transfer and melting process of PCM. The numerical results are validated against available experimental data. Then, the numerical study is extended to investigate the impacts of HTF flow parameters such as inlet temperature and mass flow rate. According to the obtained numerical results, the overall performance of the system is enhanced by increasing the inlet parameters of the HTF flow. In addition, the exergy analysis indicated that the stored exergy increases with increasing flow rate and inlet temperature of HTF. On the other hand, the exergy efficiency does not increase monotonically, but it reaches its maximum value in intermediate values of inlet flow rate and temperature.

1. Introduction

Recently, there has been significant attention on renewable energy resources in order to satisfy the growing need for energy and to reduce the dependency on the old type of energy sources like fossil fuel. One of these energies is solar power, although the main problem in using this energy is the availability problem. Therefore it is crucial to design storage unit for these systems. The most important role of the storage system is to overcome the difference between supply and demand at a different time of day [1-3]. By using PCM's as a storage medium, it is possible to store 5 to 14 times energy in comparison to other materials like water, rock, etc. in constant volume [4]. One of the most important benefits of using PCMs as a storage unit is their capability of energy delivery at a relatively constant temperature. But, the main problem in using these materials is their relatively low heat conduction which necessitates a long time for restoring energy [5].

Heat storage units are categorized into active and passive systems. In active systems, the heat transfer fluid is driven through the system by

means of a mechanical device. On the contrary, in passive systems, there are no mechanical parts and heat transfer fluid flows due to natural convection generated by temperature difference in the system [6]. Active systems themselves are divided into two categories, direct and indirect. In direct systems, heat transfer fluid itself works as a storage medium, but in indirect systems, other materials are present as a storage medium [2].

It is already proven that during the melting process heat is transferred by means of two heat transfer mechanisms: conduction and natural convection [7]. Melting process is divided into two different types - constrained and unconstrained - regarding the relative location of PCM and heat source. In the unconstrained melting process, solid PCM is placed below the heat source, and therefore the main heat transfer mechanism is conduction [8, 9]. On the contrary, in constrained melting, the solid PCM is on top of the heat source. In this melting process, conduction heat transfer is only dominant in the initial stage of melting. As the time passes, the melted fraction is increased leading to the dominance of natural convection. Thus, the overall melting and storing energy rate are higher in comparison to unconstrained melting [10].

Several studies are performed on melting process of PCM in different energy storage applications. Waqas and Ji [11] reviewed various utilization forms of phase change materials in residential cooling systems. Novel designs of solar collectors with PCM integrated as energy storage purposes have been presented and discussed by Khan and Ibrahim [12]. Al-Abidi and Mat [13] conducted an experimental study on the utilization of PCM in triplex tube heat exchangers with radial fins placed in the PCM side. Tao and He [14] employed a simplified enthalpy method to investigate thermal performance of PCM inside a shell and tube heat exchanger under non-steady inlet conditions.

Geometrical optimization of the PCM confinement has been considered as an effective parameter on thermal performance of the energy storage system. Adding fins, for example, is proven to be an efficient way in improving heat transfer and thus expedition of PCM melting process, as shown in the numerical research of Ye [15]. Also, Jahangiri and Ahmadi [16] studied the influence of internal fins in the melting process of PCM through varying fin shape factors. The impact of container orientation and inclination on the PCM melting rate has also been a matter of interest for researchers [17, 18]. Darzi and Jourabian [19] researched the influence of HTF tube location, as another influential geometrical factor, on the melting process of PCM. Talebizadeh Sardari and Walker [20] studied the impact of storage size on the thermal characteristics of composite metal foam-PCM system. Gurel [21] investigated the effect of wall thickness and HTF inlet temperature on melting rate of PCM in a plate heat exchanger. He concluded that decreasing wall thickness and increasing inlet temperature enhance melting rate significantly. In addition, he proposed an optimum design for his specific case. Mustafa et al. [22] performed a numerical study on melting rate of PCM in a double pipe helical coil system with innovative design. They investigated different parameters along HTF inlet temperature on melting rate of PCM and concluded that with the optimum design, melting time can be reduced up to 26 percent.

Thermodynamic and physical properties of PCM are also expected to play an important role in determining thermal attributes of energy storage units. Panchabikesan and Swami [23] investigated the impact of conduction coefficient of PCM on melting rate in a variety of HTF inlet temperatures and flow rates. Parsazadeh and Duan [24] conducted a numerical research on the effect of adding nanoparticle to PCM and HTF in different inlet temperatures on the melting rate of PCM. Bashar and Siddiqui [25] studied the transient behavior of the PCM in its melting process with the addition of nanoparticles. Wang and Wang [26] evaluated a composite of cascaded PCMs for its capabilities in thermal energy storage.

This paper examines the effect of inlet temperature and flow rate of PCM on the melting process with focusing on melting front and transient behavior of heat transfer mechanisms. Moreover, a second law analysis is conducted for all of the studied cases to compare their

performance regarding exergy efficiency. At first, the performance of the computational model generated for our numerical study is tested and validated against the data available in the experimental study of Bashar and Siddiqui [25]. The obtained numerical results represent a detailed three-dimensional reproduction of the PCM melting process witnessed in the experimental examination of Bashar and Siddiqui [25]. After the accomplishment of the validation phase, the numerical study is extended to investigate the effects of inlet parameters on heat transfer, melting characteristics, and exergy efficiency of thermal energy storage system.

2. Governing equations

In the current numerical investigation, Enthalpy-Porosity model of Brent and Voller [27] was used for modeling the melting process. The governing equations for transient three-dimensional simulation of heat-transfer in a PCM based thermal energy storage system are as follows.

$$\frac{\partial \rho}{\partial t} + \nabla.(\rho \mathbf{V}) = 0 \tag{1}$$

$$\rho \frac{\partial \mathbf{V}}{\partial t} + \rho \mathbf{V}.(\nabla \mathbf{V}) = -\nabla p + \mu \nabla^2 \mathbf{V} + \rho \mathbf{g}(T - T_{ref}) + \frac{C\mathbf{V}(1-\lambda)^2}{\lambda^3 - \varepsilon} \tag{2}$$

$$\frac{\partial H}{\partial t} + \nabla.(\mathbf{V}H) = \nabla.(\frac{k}{\rho C_p} \nabla h) \tag{3}$$

In Eqs. (1 to 3), V, μ, P, and ρ ąrepresent velocity vector, viscosity, pressure, and material density, respectively. C indicates mushy zone parameter which is set to a value between 10^5 and 10^6 in most studies. Also, ε is a C_p is the specific heat in constant pressure. In addition, L in Eq. (4) indicates latent heat and λ is liquid fraction, computed as follows:
small number considered to avoid division by zero. Also, H indicates enthalpy and it is computed as follows:

$$H = H_{ref} + \int_{T_{ref}}^{T} C_p dT + \lambda L \tag{4}$$

$$\lambda = \begin{cases} 0 & T \le T_s \\ \frac{T - T_{solid}}{T_l - T_{solid}} & T_s \le T \le T_l \\ 1 & T \ge T_l \end{cases} \tag{5}$$

3. Numerical model and validation

A geometric model of the thermal system under study is visualized in Fig. 1. This system is considered to be indirect since HTF is different in material composition from that of the storage medium. Polyfin is used as PCM with its relevant thermo physical properties given in Table 1. Also, air is used as HTF flowing in a copper tube with a diameter of 2.43 mm and a thickness of 0.344 mm. The PCM is stored in a container with dimensions 100×100×12 mm.
In the experimental study of Bashar and Siddiqui [25], air enters the HTF tube with a volumetric flow rate of 40 liters per minute flow rate, a density of 2.143 kg/m3 and an inlet temperature of 150°C. The Reynolds number of HTF flow is calculated to be 11200, indicating a turbulent flow regime in the HTF tube. Turbulence effects are taken into account using k-ε RNG model with enhanced wall treatment. SIMPLE algorithm is used to solve pressure-velocity coupling. In addition, all walls surrounding the domain are considered to be thermally isolated. The initial temperature of PCM is set to be 300 K and all walls of PCM container except top wall, are considered to be insulated. The isothermal boundary condition with a temperature of 27^{0c} is inserted on the top wall. No slip boundary condition is inserted on all walls of the container. The grid generated to cover the numerical domain is shown in Fig. 2. Grid independency of the numerical results is depicted in Fig. 3.

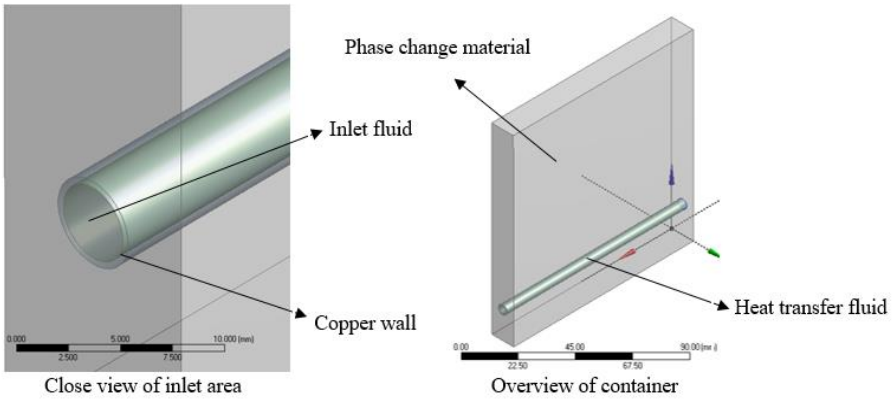

Fig. 1. Schematic of phase change material container.

Table 1. Thermophysical properties of polyfin [25].

Melting temperature °C	Specific gravity	Specific heat $kJ.kg^{-1}.K^{-1}$	Thermal conductivity $W.m^{-1}.K^{-1}$		Kinematic viscosity $m^2.s^{-1}$	Latent heat $kJ.kg^{-1}$	Thermal diffusivity $m^{-2}.s$
			Solid state	Liquid state			
55	0.92	2.89	0.24	0.18	5.5×10^{-6}	180	7.985×10^{-8}

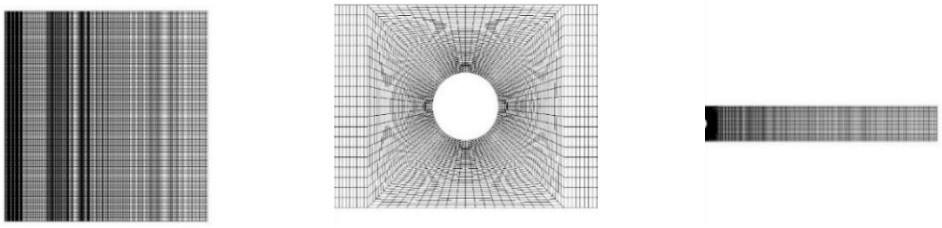

Fig. 2. Schematic of generated grid for current study.

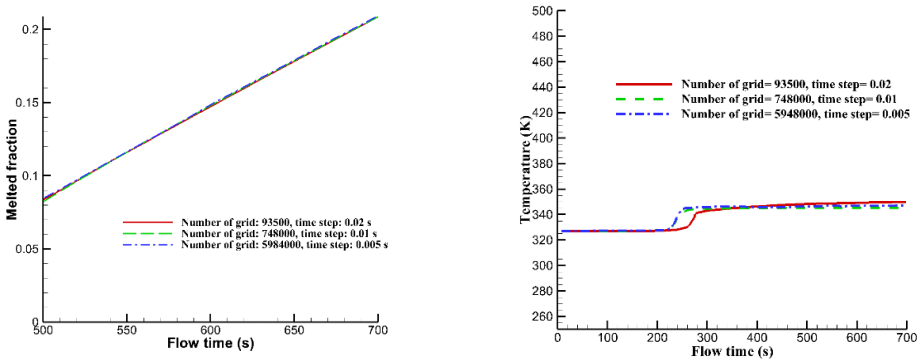

(a) (b)

Fig. 3. Grid study for (a) liquid fraction of phase change material, and (b) temperature profile for 10mm above heat transfer fluid tube.

Variations in liquid fraction and temperature of a probe located at 10mm above HTF tube are shown for three different grid resolutions. No tangible difference can be witnessed between the results of the two higher grid resolutions. Thus, 748000 grid with 0.01s time step was used for numerical simulation of all cases.

To validate our numerical model, the non-dimensional temperature profiles obtained in two different points above the HTF tube are compared with the experimental data of Bashar and Siddiqui [25]. The non-dimensional temperature used in this comparison is defined as follows:

$$\theta = \frac{T - T_m}{T_{sur} - T_m} \tag{6}$$

In this equation, T is the static temperature, T_m is the melting point temperature, and T_{sur} represents the surface temperature. The surface temperature is averaged over five probes placed in the equal distances along the HTF tube.

As shown in Fig. 4, the numerical and experimental data are in very good agreement. In addition, the evolution of the melting front was visualized and compared with the experimental data in Fig. 5. As shown in this figure, the location and orientation of the melting front predicted by the numerical model is nearly coincident with those witnessed in the experimental study of Bashar and Siddiqui [25]. The results exhibited in Figs. 4 and 5 indicate an accurate numerical prediction of melting process observed in the experimental study. Therefore, the performance of the numerical solver is validated.

4. Results and discussion

After validating the numerical algorithm in the previous section, in this section numerical results are presented and discussed. The effect inlet conditions, specifically mass flow rate and inlet temperature, on melting behavior and heat transfer mechanism is studied. Three different flow rates of 20, 40, and 80 liters per minute are considered for HTF flow. Also, inlet temperatures of HTF flow are set to be 100, 150, and 180°C. Fig. 6 shows temperature distributions in the middle vertical plane during the melting process, for all cases. The results are exhibited at three separate columns, each referring to a specific simulation time. The simulation times are 400s, 800s, and 1200s for column numbers 1 to 3, respectively. The results indicate a uniform temperature distribution in the melted region. This is mainly due to the presence of natural convention in these parts where the PCM thermodynamic state is changed to liquid. In contrast, there exists a thin hot temperature film in the solid region next to the phase interface. Here, heat conduction is the main heat transfer mechanism, inducing a temperature gradient in the vicinity of the melting front.

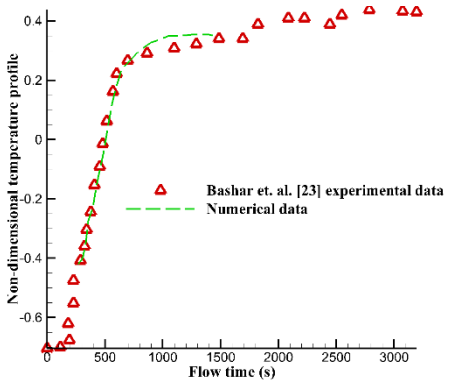

(a) 1mm above heat transfer fluid tube

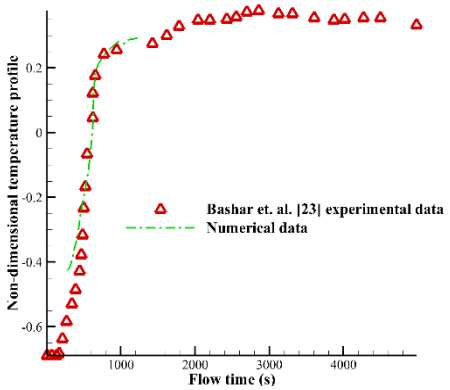

(b) 2.5mm above heat transfer fluid tube

Fig. 4. Validation results for different points.

Fig. 7 shows the 3D melting front for all of the specified inlet conditions. Columns 1, 2, and 3 in this figure correspond to simulation times 400s, 800s, and 1200s, respectively. As can be seen in this figure, melting front development below the heat source is considerably lower than the zone above the heat source. This is because of the constrained melting process in which natural convection is insignificant. Also, a slope is witnessed in the melting front from the entrance to the outlet of the HTF tube. This slope is formed because the HTF temperature gradually decreases in the flow direction.

As anticipated, with increasing the inlet flow temperature, the melted region grows more rapidly (Fig. 7 (a to c)). Moreover, the melting process is expedited when the inlet flow rate of HTF is increased at a constant inlet temperature of 150°C (Fig. 7 (b, d, and e)). It is interesting to note that the melting front is not observed at inlet flow rate of 20 liter/min, even at the latest simulation times. This indicates that the melting process has not been triggered even at simulation time 1200s for this HTF flow rate. Generally, meting front position and orientation is in accordance with the temperature jump curve witnessed in Fig. 6.

Fig. 8 shows the temperature variation along the tube centerline at different times. The axial temperature gradient is seen to be decreased in later times compared to the initial stages. This can be attributed to the melting front evolution with the passage of time. According to Fig. 7(b), in the initial time stages when melting front is situated in the vicinity of the tube, specifically near the outlet side, the surrounding PCM temperature is still relatively low. Thus, a larger fraction of the thermal energy entered into the domain is transferred to the PCM. As the time passes, the melting front advances deeper in the PCM. Thus, the HTF tube is surrounded by the melted PCM with a more uniform temperature distribution. This, in turn, causes a drop in the temperature gradient of the HTF along the centerline.

Fig. 9 shows the non-dimensional temperature profile versus time for all cases. The non-dimensional temperature profile is plotted for four points above the HTF tube with different distances. As shown in this figure, at the initial stage of the melting process, the temperature rise is generally slow for all points since the melting front is far from them. As the time passes, the melted region expands and the points become located in the thin film region of the melting front, causing a steep temperature rise in the probing points. As the melting front passes each probing point, the non-dimensional temperature value changes its sign. The temperature rate is preserved for a short time interval before it reaches its steady value. This steady temperature value is reached when the melting front is well beyond the probing point.

Moreover, at the minimum inlet temperature of HTF (100◦C), the temperature rise in PCM is significantly delayed and decreased compared to the rest cases. Decreasing the HTF flow rate to 20 liters/second while maintaining the inlet temperature at 150◦C, also results in a discernible delay in the temperature rise. Increasing the mass flow rate inlet temperature, while the other inlet parameters are maintained, constant does not lead to a significant change in temperature rise.

Fig. 10 shows the convection heat transfer coefficient (h) versus melted fraction for all examined cases. The heat transfer coefficient is defined as follows.

$$h = \frac{q}{T_{PCM} - T_{sur}} \tag{7}$$

In this equation, q is the heat transferred from HTF to PCM. T_{PCM} and T_{sur} indicate PCM bulk temperature and average temperature at the surface of the HTF tube, respectively. As can be seen in this figure, the convective heat transfer coefficient (h) decreases with increasing melted fraction for all simulation cases. The results are seen to be in reasonable agreement with the experimental data.

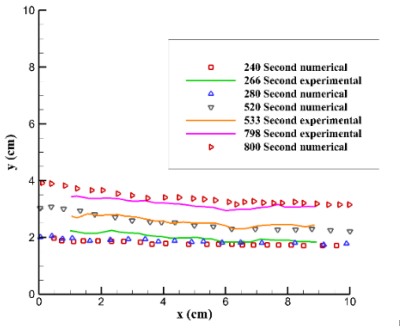

Fig. 5. Melting front position in the vertical middle plane.

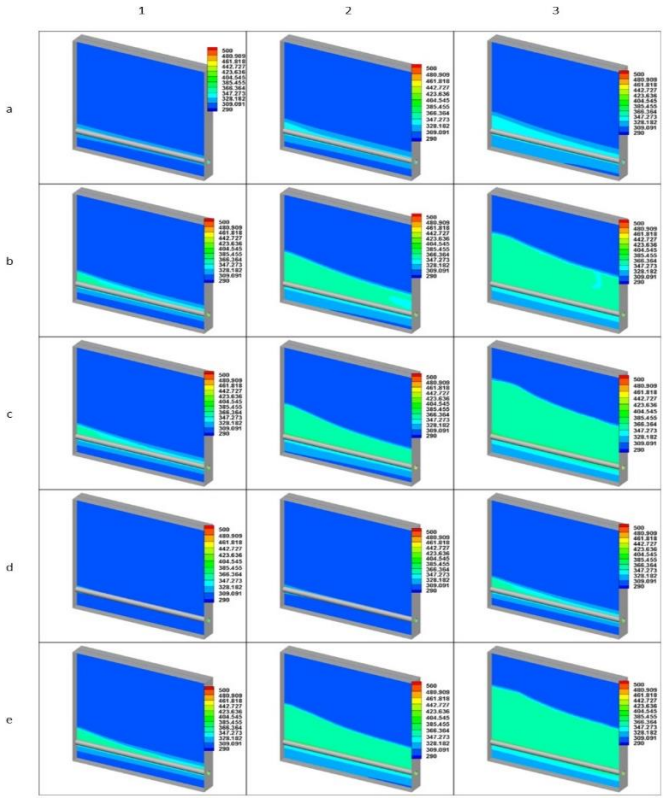

Fig. 6. Temperature distribution for inlet temperature (°C) and flow rate (liter/min) equal to (a) 100 and 40, (b) 150 and 40, (c) 180 and 40, (d) 150 and 20, (e) 150 and 80.

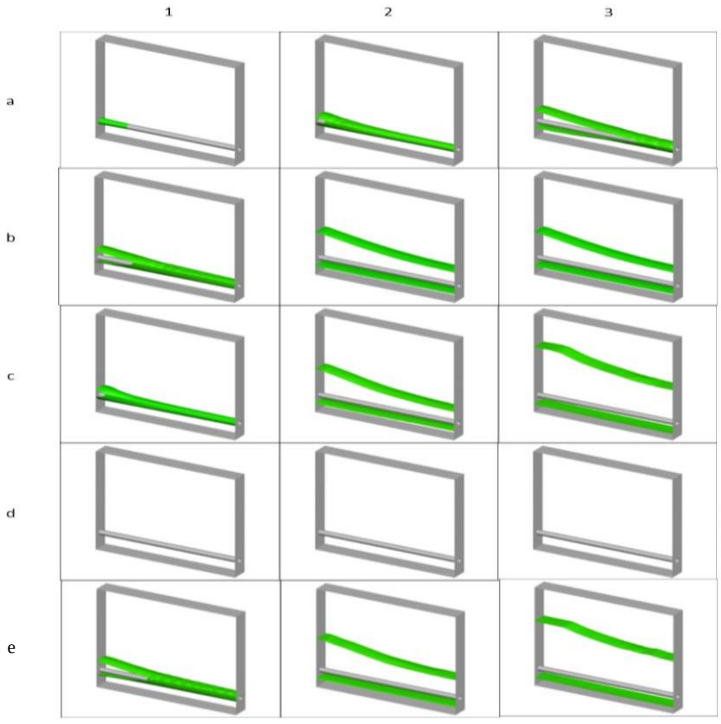

Fig. 7. 3D melting front for inlet temperature (°C) and flow rate (liter/min) equal to (a) 100 and 40, (b) 150 and 40, (c) 180 and 40, (d) 150 and 20, (e) 150 and 80.

It is noticed that h varies sharply with variations in volume fraction in low values of volume fraction. However, in the higher melted fractions when the melting front is far away from the heat source, the temperature in the PCM surrounding the HTF tube is nearly uniform. On the other hand, the temperature gradient normal to the HTF tube reaches a constant level. Thus, the heat transfer coefficient value remains nearly constant in higher melted fractions. This trend is similar for all cases. Furthermore, the final heat transfer value increases with increasing either inlet temperature or HTF flow rate. This occurs because of the increase in thermal energy input in both cases. In the last part of this section, exergy efficiency of the presented thermal system is investigated for all inlet conditions. In order to do so, stored and inlet exergy are computed as follows.

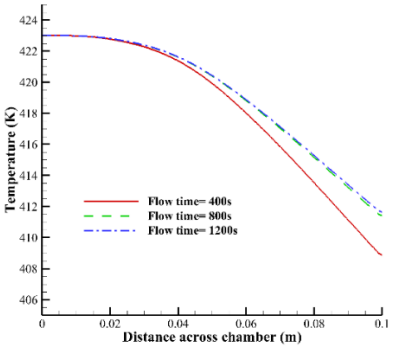

Fig. 8. Heat transfer fluid temperature gradient along the tube centerline at an inlet temperature of 150 °C and a heat transfer fluid flow rate of 40 liter/min.

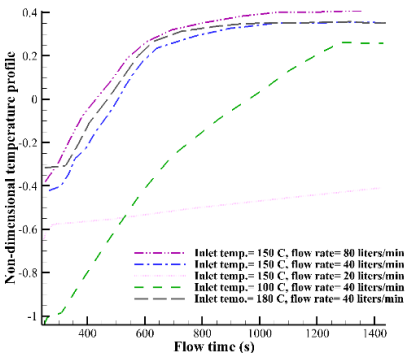

(a) 1 mm above heat transfer fluid tube

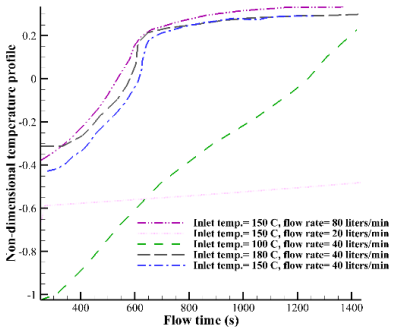

(b) 2.5 mm above heat transfer fluid tube

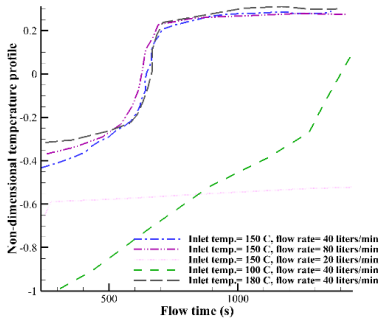

(c) 5 mm above heat transfer fluid tube

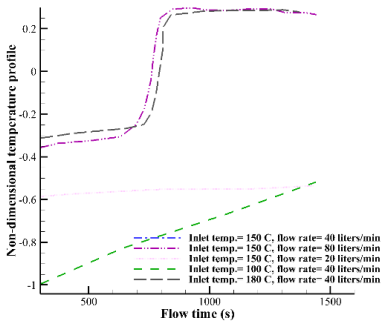

(d) 10 mm above heat transfer fluid tube

Fig. 9. Non-dimensional temperature profile for different points in all cases.

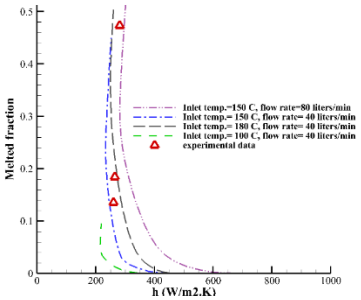

Fig. 10. Melted friction respected to connective heat transfer coefficient (h) for all investigated cases.

$$ex_{PCM} = \begin{cases} \rho C_{p,PCM}[(T - T_{init}) - T_0 \ln(\frac{T}{T_0})] & if\ (T < T_m) \\ \rho C_{p,PCM}[(T_m - T_{init}) - T_0 \ln(\frac{T_m}{T_{init}})] + \rho L(1 - \frac{T_0}{T_m}) & \\ + \rho C_{p,PCM}[(T - T_m) - T_0 \ln(\frac{T}{T_m})] & if\ (T > T_m) \end{cases} \quad (8)$$

$$EX_{PCM} = \int ex_{PCM}\, dV \quad (9)$$

$$EX_{input} = \int \dot{m}_{HTF} C_{p,HTF}[(T_{HTF,in} - T_{HTF,out}) - T_0 \ln(\frac{T_{HTF,in}}{T_{HTF,out}})]dt \quad (10)$$

In Eqs. (8-10), $C_{P,PCM}$ and $C_{P,HTF}$ show PCM and HTF specific heat, respectively. Also, $T_{HTF,in}$ and $T_{HIF,out}$ show HTF inlet and outlet temperature, respectively. In addition, m_{HTF} shows HTF flow rate, T_0, T_m, , and T_{init} are ambient temperature, melting temperature, and initial temperature, respectively. Then exergy storage efficiency is defined to be the ratio of the stored exergy to the inlet exergy.

Fig. 11 shows the second law analysis of the PCM. Increment in exergy storage is plotted against time in Fig. 11(a). As can be expected, the rise in exergy input is expedited with increasing inlet temperature or HTF flow rate. Specifically, in the cases with minimum HTF flow rate or minimum inlet temperature, the rate of exergy storage is considerably lower compared to other cases. This is due to the significant delay in the melting process. Based on Eq. (10), the exergy is mostly stored in the PCM during the phase change process. Thus, in cases with lower phase change rate, the most significant term $(\rho L(1 - \frac{T_0}{T_m}))$ could not contribute effectively in the exergy storage.

Fig. 11(b) indicates exergy efficiency versus time. The exergy efficiency of the case with HTF inlet temperature of 150◦C and HTF flow rate of 40 liters per minute is distinguishably increased compared to the cases with higher HTF inlet temperature or mass flow rate. This shows in these cases, the absorbed exergy does not increase with the same rate as that of the input exergy. Thus, a decrease in exergy efficiency has resulted in cases with higher inlet temperature and HTF flow rate.

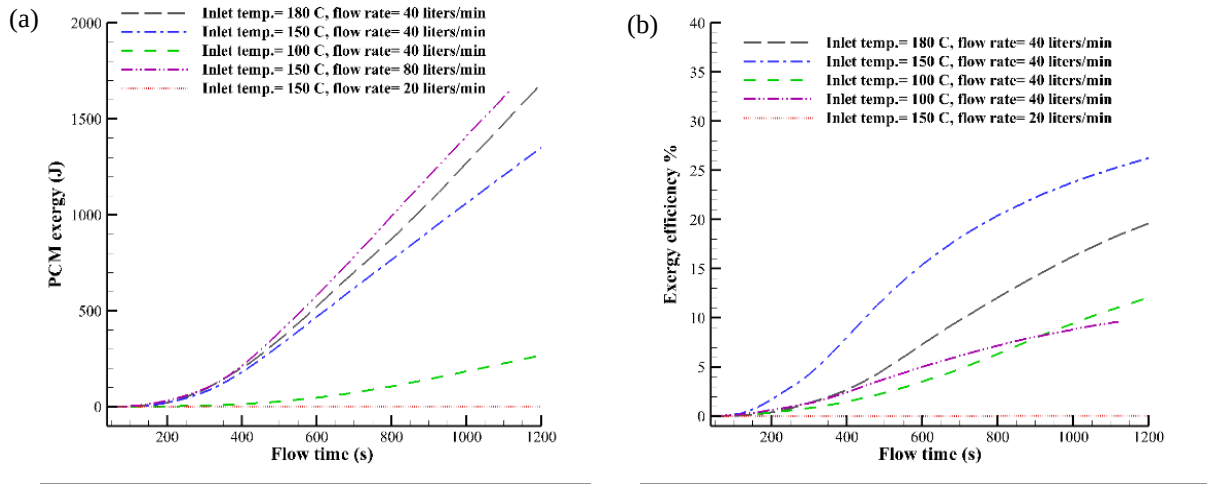

Fig. 11. Exergy analysis of the thermal system (a) Stored exergy by phase change material, and (b) Exergy storage efficiency.

5. Conclusions

The current study evaluates the effect of heat transfer fluid inlet temperature and flow rate on the melting process. The obtained results were validated against the available experimental data. Then, the effects of the mentioned parameters on the heat transfer and phase change characteristics were studied. With increasing inlet temperature or flow rate of the HTF, melting process was seen to be expedited resulting into higher thermal energy storage. Also, exergy analysis was performed for all cases with different inlet conditions. Exergy analysis showed that increasing HTF flow rate or temperature, although increasing the exergy stored in the system, does not necessarily increase the exergy efficiency.

Acknowledgement

The support and resources from the Center for High Performance Computing (SARMAD) at the Shahid Beheshti University are acknowledged.

References

[1] H. Mehling, and L. F. Cabeza, *Heat and cold storage with PCM*, springer, (2008).

[2] L. F. Cabeza, “Advances in thermal energy storage systems: Methods and applications”, *Adv. Therm. Energy Storage Syst.*, pp. 37-54, (2021).

[3] S. Kakac, Y. Yener, and A. Pramuanjaroenkij, *Convective heat transfer*, (2013).

[4] A. Sharma, V. V. Tyagi, C. R. Chen, and D. Buddhi, “Review on thermal energy storage with phase change materials and applications”, *Renewable Sustainable Energy Rev.*, Vol. 13, No. 2, pp. 318-345, (2009).

[5] S. Jegadheeswaran, and S. D. Pohekar, "Performance enhancement in latent heat thermal storage system: a review", *Renewable Sustainable Energy Rev.*, Vol. 13, No. 9, pp. 2225-2244, (2009).

[6] M. M. Farid, A. M. Khudhair, Sak Razack, "A review on phase change energy storage: materials and applications", *Energy Convers. Manage.*, Vol. 45, No. 9-10, pp. 1597-1615, (2004).

[7] N. I. Ibrahim, F. A. Al-Sulaiman, and S.Rahman, "Heat transfer enhancement of phase change materials for thermal energy storage applications: A critical review", *Renewable Sustainable Energy Rev.*, Vol. 74, pp. 26-50, (2017).

[8] M. Rizan, F. Tan, and C. P. Tso, "An experimental study of n-octadecane melting inside a sphere subjected to constant heat rate at surface", *Int. Commun. Heat Mass*, Vol. 39, No. 10, pp. 1624-1630, (2012).

[9] F. Tan, "Constrained and unconstrained melting inside a sphere", *Int. Commun. Heat Mass*, Vol. 35, No. 4, pp. 466-475, (2008).

[10] F. Tan, et al., "Experimental and computational study of constrained melting of phase change materials (PCM) inside a spherical capsule", *Int. J. Heat Mass Transfer.*, Vol. 52, No. 15-16, pp. 3464-3472, (2009).

[11] A. Waqas, et al., "Effectiveness of the phase change material-based thermal energy storage integrated with the conventional cooling systems of the buildings–A review", *Proc. Inst. Mech. Eng. Part: A, J. Power Energy.*, Vol. 232, No. 6, pp. 735-766, (2018).

[12] M. M. A. Khan, N. I. Mahbubul, H. M. Ali, and R. Saidur, "Evaluation of solar collector designs with integrated latent heat thermal energy storage: a review", *Sol. Energy.*, Vol. 166, pp. 334-350, (2018).

[13] A. A. Al-Abidi, S. Mat, K. Sopian, and M. Y. Sulaiman, "Experimental study of melting and solidification of PCM in a triplex tube heat exchanger with fins", *Energy. Build.*, Vol. 68, pp. 33-41, (2014).

[14] Y. Tao, and Y. He, "Numerical study on thermal energy storage performance of phase change material under non-

steady-state inlet boundary", *Appl. Energy.*, Vol. 88, No. 11, pp. 4172-4179, (2011).

[15] W. B. Ye, "Enhanced latent heat thermal energy storage in the double tubes using fins", *J. Therm. Anal. Calorim.*, Vol. 128, No. 1, pp. 533-540, (2017).

[16] A. Jahangiri, and O. Ahmadi, "Numerical investigation of enhancement in melting process of PCM by using internal fins", *J. Therm. Anal. Calorim.*, Vol. 137, No. 6, pp. 2073-2080, (2019).

[17] B. Kamkari, and H. Shokouhmand, "Experimental investigation of phase change material melting in rectangular enclosures with horizontal partial fins", *Int. J. Heat Mass Tran.*, Vol. 78, pp. 839-851, (2014).

[18] B. Kamkari, and H. J. Amlashi, "Numerical simulation and experimental verification of constrained melting of phase change material in inclined rectangular enclosures", *Int. Commun. Heat Mass*, Vol. 88, pp. 211-219, (2017).

[19] A. A. R. Darzi, M. Jourabian, and M. Farhadi, "Melting and solidification of PCM enhanced by radial conductive fins and nanoparticles in cylindrical annulus", *Energy Convers. Manage*., Vol. 118, pp. 253-263, (2016).

[20] P. Talebizadeh Sardari, and G. S. Walker, "Numerical modelling of phase change material melting process embedded in porous media: Effect of heat storage size", *Proc. Inst. Mech. Eng. Part: A, J. Power Energy.*, Vol. 234, No. 3, pp. 365-383, (2020).

[21] B. GÜREL, "A numerical investigation of the melting heat transfer characteristics of phase change materials in different plate heat exchanger (latent heat thermal energy storage) systems", *Int. J. Heat Mass Transfer.*, Vol. 148, p. 119117, (2020).

[22] M. S. Mahdi, H. B. Mahood, J. M. Mahdi, A. A. Khadom, "Improved PCM melting in a thermal energy storage system of double-pipe helical-coil tube", *Energy Convers. Manage.*, Vol. 203, pp. 112238, (2020).

[23] K. Panchabikesan, et al., Influence of PCM thermal conductivity and HTF velocity during solidification of PCM through the free cooling concept–A parametric study. *J. Energy Storage*, Vol. 21, pp. 48-57, (2019).

[24] M. Parsazadeh, and X. Duan, "Numerical and statistical study on melting of nanoparticle enhanced phase change material in a shell-and-tube thermal energy storage system", *Appl. Therm. Eng.*, Vol. 111, pp. 950-960, (2017).

[25] M. Bashar, and K. Siddiqui, "Experimental investigation of transient melting and heat transfer behavior of nanoparticle-enriched PCM in a rectangular enclosure", *J. Energy Storage*, Vol. 18, pp. 485-497, (2018).

[26] Y. Wang, et al., "Numerical study on thermal performance characteristics of a cascaded latent heat storage unit", *Proc. Ins. Mech. Eng. Part: A, J. Power Energy*, Vol. 230, No. 1, pp. 126-137, (2016).

[27] A. Brent, V. R. Voller, and K. Reid, "Enthalpy-porosity technique for modeling convection-diffusion phase change: application to the melting of a pure metal". *Numer. Heat Transfer Part: A, Appl.*, Vol. 13, No. 3, pp. 297-318, (1988).

How to cite this paper:

Omid Ahmadi, Sahand Majidi and Pooyan Hashemi Tari, "Numerical study of transient behavior and heat transfer in a phase change material (PCM) affected by heat transfer fluid (HTF) flow parameters", *J. Comput. Appl. Res. Mech. Eng.*, Vol. 10, No. 2, pp. 461-472, (2021).

DOI: 10.22061/jcarme.2020.5941.1754

URL: https://jcarme.sru.ac.ir/?_action=showPDF&article=1226